HHS Public Access

Author manuscript

Lab Invest. Author manuscript; available in PMC 2009 October 01.

Published in final edited form as:

Lab Invest. 2009 April ; 89(4): 456–469. doi:10.1038/labinvest.2009.6.

Morphological and Functional Heterogeneity of the Mouse Intrahepatic Biliary Epithelium

Shannon Glaser, Ph. D.[2,3,#], **Eugenio Gaudio, M. D.**[9,#], **Arundhati Rao, M.D., Ph. D.**[6], **Lisa Pierce, Ph. D.**[5], **Paolo Onori, M. D.**[10], **Antonio Franchitto, B. S.**[9], **Heather Francis, B. S.**[3,8], **David E Dostal, Ph.D.**[1,7], **Julie Venter, B. S.**[3], **Sharon DeMorrow, Ph. D.**[2,3], **Romina Mancinelli, Ph. D.**[2,9], **Guido Carpino, M. D.**[11], **Domenico Alvaro, M. D.**[12], **Shelley Kopriva, B. S.**[1], **Jennifer Savage, B. S.**[3], and **Gianfranco Alpini, Ph. D.**[1,2,3,4]

[1]From Research, Central Texas Veterans Health Care System

[2]Scott & White Digestive Diseases Research Center, Temple, TX

[3]Department Medicine and Scott & White and Texas A&M Health Science Center, College of Medicine, Temple, TX 76504

[4]Systems Biology and Translational Medicine, Scott & White and Texas A&M Health Science Center, College of Medicine, Temple, TX 76504

[5]Obstetrics and Gynecology, Scott & White and Texas A&M Health Science Center, College of Medicine, Temple, TX 76504

[6]Technical Pathology and Molecular Genetics, Pathology, Scott & White and Texas A&M Health Science Center, College of Medicine, Temple, TX 76504

[7]Molecular Cardiology, Scott & White, Temple, TX 76504

[8]Division of Research and Education, Scott & White, Temple, TX 76504

[9]Department of Anatomy, University of Rome, Italy

[10]Department of Experimental Medicine, University of L'Aquila, L'Aquila, Italy

[11]Dept Health Science, IUSM, University of Motor Sciences, Rome, Italy

[12]Department of Gastroenterology, University of Rome, Italy.

Abstract

Rat and human biliary epithelium is morphologically and functionally heterogeneous. Since no information exists on the heterogeneity of the murine intrahepatic biliary epithelium, and with

Address correspondence to: Shannon Glaser, Ph.D. Assistant Professor Scott and White Hospital and Texas A&M Health Science Center College of Medicine 702 SW H.K. Dodgen Loop, Temple, TX, 76504 Phone: 254-742-7058 Fax: 254-724-5944 Email: sglaser@tamu.edu or Gianfranco Alpini, Ph. D. VA Research Scientist Career Award Recipient Professor, Medicine and Systems Biology and Translational Medicine Dr. Nicholas C. Hightower Centennial Chair of Gastroenterology Director of the Scott & White Digestive Diseases Research Center Research, Central Texas Veterans Health Care System Scott & White and Texas A & M Health Science Center College of Medicine Medical Research Building 702 SW H.K. Dodgen Loop, Temple, TX, 76504 Phone: 254-742-7044 or 254-742-7046 Fax: 254-724-9278 or 254-724-5944 E-mail: galpini@tamu.edu or galpini@medicine.tamhsc.edu.

[#]Dr. Glaser and Prof. Gaudio contributed equally to this manuscript.

increased usage of transgenic mouse models to study liver disease pathogenesis, we sought to evaluate the morphological, secretory and proliferative phenotypes of small and large bile ducts and purified cholangiocytes in normal and cholestatic mouse models.

Methods—For morphometry, normal and BDL mouse livers (C57/BL6) were dissected into blocks of 2-4 μm^2, embedded in paraffin, sectioned, and stained with H&E. Sizes of bile ducts and cholangiocytes were evaluated by using SigmaScan to measure the diameters of bile ducts and cholangiocytes. In small and large normal and BDL cholangiocytes, we evaluated the expression of cholangiocyte specific markers, keratin-19 (KRT19), secretin receptor (SR), cystic fibrosis transmembrane conductance regulator (CFTR), and chloride bicarbonate anion exchanger 2 (Cl^-/HCO^-_3 AE2) by immunofluorescence and western blot; and intracellular cAMP levels and chloride efflux in response to secretin (100 nM). To evaluate cholangiocyte proliferative responses after bile duct ligation (BDL), small and large cholangiocytes were isolated from BDL mice. The proliferation status was determined by analysis of the cell cycle by FACS and bile duct mass was determined by the number of KRT19-positive bile ducts in liver sections.

Results—*In situ* morphometry established that the biliary epithelium of mice is morphologically heterogeneous, which smaller cholangiocyte lining smaller bile ducts and larger cholangiocytes lining larger ducts. Both small and large cholangiocytes express KRT19 and only large cholangiocytes from normal and BDL mice express SR, CFTR, and Cl^-/HCO^-_3 exchanger and respond to secretin with increased cAMP levels and chloride efflux. Following BDL, only large mouse cholangiocytes proliferate.

Conclusion—Similar to rats, mouse intrahepatic biliary epithelium is morphologically, and functionally heterogeneous. The mouse is a suitable model for defining the heterogeneity of the biliary tree.

Keywords

Bicarbonate secretion; bile ducts; cAMP; cholangiocytes; mitosis; secretin; secretin receptor

---

In recent years, knowledge associated with biliary epithelial cell (i.e., cholangiocytes) function has been significantly enhanced due to increased interest in cholestatic liver diseases, biliary fibrosis, and biliary cancer (1-6). Cholangiocytes were originally termed as ‘simple’ epithelia, which line the intrahepatic and extrahepatic bile ducts (7-9). Despite the original terminology of ‘simple epithelia’, cholangiocytes play an important role in the modification of ductal bile, as well as in the detoxification of xenobiotics (1, 2, 10, 11). In diseases of the biliary tree (i.e., cholangiopathies) such as primary sclerosing cholangitis (PSC), primary biliary cirrhosis (PBC), liver allograft rejection and graft-versus-host disease), cholangiocytes are the target cells (1, 3). Cholangiopathies cause morbidity and mortality and are a major reason for liver transplantation (1, 3) and graft loss (12). Cholangiopathies are characterized by patchy rather than diffuse proliferation and loss of different sized ducts, which suggest that cholangiocytes are heterogeneous and respond differentially to cholestatic diseases and toxin-induced liver injury (1, 5, 13).

Recently, the concept of heterogeneity of the rat biliary epithelium has been explored (1, 5, 7, 8, 10, 13-18) and classified into three categories: (i) morphological (7, 8, 14); (ii) secretory (7, 14, 16); and (iii) proliferative (5, 10, 13, 15, 17-19). *Morphological*

heterogeneity— In humans, the biliary ductal system is classified into three different sized segments, which include the extrahepatic bile duct, large bile ducts and intrahepatic small bile ducts (1, 6, 9). The biliary system extends from the canals of Hering to the large extrahepatic ducts (1, 6, 9). In humans, the intrahepatic biliary epithelium has been divided based upon duct diameter size (1, 6, 9): small bile ductules (<15 μm), interlobular ducts (15-100 μm), septal ducts (100-300 μm), area ducts (300-400 μm), segmental ducts (400-800 μm) and hepatic ducts (> 800 μm) ducts (1, 5, 6, 9).

Small ductules are lined by four to five cholangiocytes, which are characterized by the presence of a basement membrane, tight junctions between cells and microvilli projecting into the bile duct lumen (5, 9, 20). Small bile ducts join into interlobular ducts ranging from 20-100 μm in cross-sectional diameter (5, 6, 9, 20). In large bile ducts, cholangiocytes are larger and more columnar in shape (6, 9, 20). Similar to humans, a number of *in situ* (in liver sections) and *in vitro* (in purified small and large cholangiocytes and isolated small and large intrahepatic bile duct units) studies have demonstrated that the rat intrahepatic biliary epithelium is morphologically heterogeneous (7, 8, 14).

Functional heterogeneity

Following secretion at the bile canaliculus by hepatocytes (21), cholangiocytes modify bile as it flows through the biliary tree by a series of hormone-regulated Ca^{2+}- or cAMP-dependent reabsorptive and secretory events (4, 15, 22-30). Large, cAMP-responsive rat cholangiocytes express secretin receptors (SR), CFTR and the chloride bicarbonate anion exchanger 2 (Cl^-/HCO^-_3 AE2) (7, 14, 16), whose activation leads to changes in ductal secretion of water and electrolytes including HCO^-_3 ions (7, 14, 16). Large cholangiocytes are the only cell types in the liver, which express the secretin receptor (7, 14, 16). The pathophysiology of small cholangiocytes is undefined (19).

Proliferative heterogeneity

In humans and rodent models, normal cholangiocytes are mitotically dormant (10, 31). In the human liver, cholangiocyte proliferation is observed in extrahepatic biliary obstruction; during the course of cholestatic liver diseases (e.g., PBC, PSC, liver allograft rejection, and graft-versus-host disease); and in response to alcohol, toxins, or drugs (1, 3). Similar to findings in human cholangiopathies (1, 3), cholangiocyte proliferation in the rat liver occurs within a limited range of bile duct sizes (1, 10, 31). In rats with extrahepatic cholestasis induced by BDL, enhanced cholangiocyte proliferative capacity is restricted to large bile ducts (15, 18). In this hyperplastic model, cholangiocyte proliferation is closely associated with increased SR gene expression and secretin-stimulated cAMP levels, which play a pivotal role in the modulation of cholangiocyte proliferative responses due to cholestasis (4, 15, 16, 26, 32, 33). Despite our knowledge regarding human and rat heterogeneity, information regarding the morphological, proliferative and functional heterogeneity of mouse intrahepatic biliary epithelium is limited (19). With increased availability and usage of transgenic mouse models for studying cholestatic liver disease pathogenesis, we sought to evaluate the morphological, secretory, proliferative and apoptotic phenotypes of small and large mouse bile ducts in normal and cholestatic models.

MATERIALS AND METHODS

Materials

Reagents were purchased from Sigma Chemical Co. (St. Louis, MO) unless otherwise indicated. Porcine secretin was purchased from Peninsula (Belmont, CA). The nuclear dye 4,6-diamidino-2-phenylindole (DAPI) was purchased from Molecular Probes, Inc., Eugene, OR. The secretin receptor (C-20) is an affinity purified goat polyclonal antibody (Santa Cruz Biotechnology Inc., Santa Cruz, CA) raised against a peptide mapping at the C-terminus of secretin receptor of human origin and cross-reacts with mouse (19). The CFTR monoclonal (IgG1) antibody (M3A7, Thermo Fisher Scientific, Fremont, CA) was raised against the recombinant protein encoding the nucleotide binding fold (NBF2) domain of human CFTR and cross-reacts with mouse (19). The anti Cl^-/HCO^-_3 AE2 (reacting with the chloride bicarbonate anion exchanger 2) (19) is an affinity purified rabbit anti-rat AE-2 IgG, # AE21-A, that was purchased from Alpha Diagnostic International (San Antonio, TX). The mouse anti-keratin-19 (KRT-19) antibody (clone RCK105) was purchased from Caltag Laboratories Inc. (Burlingame, CA). The RIA kits for the determination of intracellular cAMP levels were purchased from Perkin Elmer, Shelton, CT.

Animal Model

Male C57BL/6 mice were purchased from Charles River (Wilmington, MA), maintained in a temperature-controlled environment (20-22°C) with a 12-hour light-dark cycle and fed *ad libitum* standard chow. Mice had free access to drinking water. Our studies were carried out in: (i) normal mice; and (ii) mice with BDL (34, 35) for 3 and 7 days. Prior to each experimental procedure, the animals were anesthetized with sodium pentobarbital (50 mg/kg, IP). All animal experiments were performed in accordance with a protocol approved by the Scott and White Institutional Animal Care and Use Committee, and in accordance with the Guide for the Care and Use of Laboratory Animals published by the US National Institutes of Health (NIH Publication No. 85-23, revised 1996).

In Situ Morphometric Analysis of Intrahepatic Bile Ducts of Normal and BDL Mice

Morphometric analysis was performed in liver sections from normal and 3-day BDL mice to demonstrate that murine bile ducts and cholangiocytes exhibit morphological heterogeneity similar to the rat biliary epithelium (7, 8). Briefly, two mouse livers from each group were fixed with 2% paraformaldehyde. The entire livers were dissected into blocks of 2-4 μm^2, processed using standard procedures, embedded in paraffin, sectioned (5 μm), and stained for hematoxylin and eosin (H&E). Morphometrical analysis was performed utilizing a parameter (cut off level) to recognize and define small ducts as less than <15 μm and haveing a maximum number of 4 cholangiocytes lining the bile duct. Since the average diameter of a single small cholangiocyte is around 7 μm, a bile duct lined by 4 (or less) cholangiocytes should have a diameter < than 15 μm. The usage of the 4 cholangiocyte per duct parameter reduces the number errors that might be generated by the angle of the section plane. For normal mouse livers, a total of 23 small and 4 large bile ducts were measured using SigmaScan Pro 5.0 (SPSS, Inc., Chicago, IL). A total of 250 cholangiocytes were measured (60 from small bile ducts, and 113 from large ducts). For BDL mice livers, a total of 41 small, 22 dilated small and 3 large ducts were measured using SigmaScan Pro 5.0. A

total of 466 cholangiocytes were measured (84 from small ducts, 90 from dilated small ducts, 100 from intermediate ducts, 111 from large ducts, and 81 from major ducts).

Purification of Pooled, Small and Large Cholangiocytes

Following standard collagenase perfusion (36), a mixed cholangiocyte-enriched suspension was obtained from intact portal tracts of mice as described (36). The mixed cholangiocyte-enriched suspension was further separated into two distinct subpopulations of small and large cholangiocytes (97-100% pure by keratin-19 immunohistochemistry) (19, 35) by counterflow elutriation (2,500 rpm at the flow rates of 22 and 70 ml/minutes, respectively) (7, 10, 16-19) using a Beckman J2-21M centrifuge equipped with a JE-6B rotor (Beckman Instruments Inc., Fullerton, CA) (7, 10, 16-19). Following centrifugal elutriation, distinct subpopulations of small and large mouse cholangiocytes were further purified by immunoaffinity separation using a monoclonal antibody, rat IgG2a (provided by Dr. R. Faris, Providence, RI) against an antigen expressed by cholangiocytes (36). The centrifugal elutriation step was excluded for the isolation of pooled mouse cholangiocytes. To assess the degree of contamination by mesenchymal cells, we stained cytospin smears of isolated small, large and pooled mouse cholangiocytes for vimentin (16). Hepatocyte contamination was determined by histochemistry for glucose-6-phosphatase (G-6-P) (37). Before staining, the immunomagnetic beads used for the purification were detached by enzymatic digestion.

Measurement of Cell Size Distribution in Isolated Pooled, Small and Large Cholangiocytes from Normal and BDL Mice

We first determined the cell size distribution in pure pooled cholangiocytes, a fraction that includes small and large cholangiocytes (7, 16). Pooled mouse cholangiocytes were isolated from normal and 3- and 7-day BDL mice as described above (36). Small and large mouse cholangiocytes from normal and 3- and 7-day BDL mice were also evaluated (7, 16). Cytospin smears were prepared with approximately 50,000 cells per slide. Slides were mounted with 1X phosphate buffered saline (1X PBS). Digital images were obtained by light microscopy with an Olympus BX-40 (Tokyo, Japan) microscope equipped with a camera. The cell diameter of 100 to 200 cholangiocytes was determined using SigmaScan Pro 5.0. Size calibration was obtained using Polybeads (Dyed Blue 10 μm, Polyscience, Inc. Warrington, PA) as a standard. The diameter of the Polybeads was 9.91 ± 0.73 μm.

Effect of BDL on the Proliferation of Small and Large Bile Ducts and Isolated Small and Large Cholangiocytes

We next performed experiments to evaluate whether (similar to rats) (10, 15) BDL stimulates proliferation of large but not small murine cholangiocytes. Cholangiocyte hyperplasia was measured by determining the number of small (< 15 μm) (14) and large (> 15 μm) (14) bile ducts in liver sections (4-5 μm thick; 3 slides evaluated per group of animals) stained with KRT19 (35), an approach previously used by us (10). Sections were evaluated in a coded fashion using light microscopy (Nikon, Tokyo, Japan). Over 100 cholangiocytes were counted in three different fields for each group of animals.

The proliferative status of purified small and large cholangiocytes was also determined by cell cycle analysis by fluorescence activated cell sorting (FACS) (38). The cells were

dissociated in trypsin/EDTA, pelleted by centrifugation, and resuspended at approximately 10^6 cells/ml in 1X PBS containing 0.1% fetal bovine serum. The cells were fixed in 70% ice-cold ethanol, followed by incubation in nuclei staining buffer (PI/RNase Staining Buffer, BD Biosciences Pharmingen, San Diego, CA) for 30 minutes at 22°C according to the manufacturer's recommendations. Cell cycle histograms were generated after analyzing the propidium iodide-stained cells by FACS (FACSCalibur, BD Biosciences), in which 10^4 events were recorded for each sample. The samples were analyzed using CellQuest Pro software (BD Biosciences, San Jose, CA). Cells (1×10^6) were stained with 0.5 ml propidium iodide/RNAse staining buffer (50 μg/ml propidium iodide, 200 μg/ml DNAse-free RNAse in 1× PBS containing 0.1% Triton X-100) for 30 minutes at room temperature and analyzed in the FL3 channel using flow cytometry. The percentage of cells in Go/G1, S and G2/M phases of the cell cycle were determined using software analysis (Modfit LT 3.0, Verify Software House, Topsham, ME). Analysis was performed on singlets, in which cell aggregates were eliminated by gating FL3-Width versus FL3-Area.

Expression of SR, CFTR, Cl^-/HCO^-_3 AE2 and KRT19 in Small and Large Bile Ducts in Liver Sections, and Purified Small and Large Cholangiocytes

We evaluated the expression of SR, CFTR, Cl^-/HCO^-_3 AE2 and KRT19 by: (i) immunohistochemistry in paraffin-embedded liver sections (4-5 μm thick; 3 slides evaluated per group of animals); and (ii) immunofluorescence (19) in purified small and large cholangiocytes from normal, 3- and 7-day BDL mice.

Immunohistochemistry in Liver Sections—Liver sections were mounted on glass slides coated with acetone aminopropyltriehoxylan (2%) solution. After deparaffination, endogenous peroxidase activity was blocked by incubation (30 minutes) in methanolic hydrogen peroxide (2.5%). Sections were hydrated in graded ethanol and rinsed in 1X PBS. The endogenous biotin was blocked by the Biotin Blocking System (Dako Cytomation, Glostrup, Denmark). Following washes in 1X PBS, sections were incubated overnight at 4°C with selected primary antibody (1:100 dilution). Samples were rinsed with 1X PBS, incubated for 10 minutes at room temperature with a secondary biotinylated antibody (Dako Cytomation LSAB Plus System-HRP), then with Dako ABC (Dako Cytomation LSAB Plus System-HRP), developed with 3-3′ diaminobenzidine and counterstained with haematoxylin. For all immunoreactions, negative controls (with pre-immune serum substituted for the primary antibody) were included. Blinded observations and light microscopy photographs of liver sections were taken by Leica Microsystems DM 4500 B Light Microscopy (Weltzlar, Germany) with a Jenoptik Prog Res C10 Plus Videocam (Jena, Germany). When 0-5% of bile ducts were positive for SR, CFTR or Cl^-/HCO^-_3 AE2, we assigned a negative score; a +/- score was assigned when 6-10% of bile ducts were positive; a + score was assigned when 11-30% of bile ducts were positive; a ++ score was assigned with 31-60% of bile ducts positive; and a score +++ was assigned when more than 61% of bile ducts were positive. Three pathologists in a blinded fashion independently performed the evaluations.

Immunofluorescence in Small and Large Mouse Cholangiocytes—Cytospin smears of purified small and large mouse cholangiocytes were prepared with approximately 50,000 cells per slide. The slides were fixed in ice-cold acetone and placed in 1X PBS and

washed for 5 minutes at room temperature. Next, the slides were washed three times for 10 minutes each at room temperature in PBST (1X PBS with 0.2% Triton X100) and blocked 1 hour at room temperature in 4% BSA in 1X PBS. The blocking solution was removed and the cover slips were incubated for 24 hours 4°C with the primary antibodies diluted in 1% BSA/PBS. Primary antibodies against the following proteins were used: KRT19, SR, CFTR or Cl^-/HCO^-_3 AE2. The next day, slides were washed 3 times for 10 minutes at room temperature in PBST. Next, slides were incubated with Cy3-conjugated anti rabbit secondary antibody 1:50 (Jackson Immunochemicals, West Grove, PA) in 1% BSA/PBS at room temperature for 2 hours and washed three times for 10 minutes each with PBST. Following incubation, slides were washed 3 times for 10 minutes each in PBST at room temperature and mounted into microscope slides with Antifade gold containing 4,6-diamidino-2- phenylindole (DAPI) as a counterstain (Molecular Probes, Eugene, OR). Negative controls (with pre-immune serum substituted for the primary antibody) were also included. Images were taken on an Olympus IX71 fluorescence microscope with a DP70 digital camera.

Effect of Secretin on Intracellular cAMP Levels and Cl^- Efflux in Freshly Isolated Small and Large Mouse Cholangiocytes

Intracellular cAMP Levels—We next evaluated the effects of secretin (100 nM) (7, 16, 32, 39) on intracellular cAMP levels (7, 16, 26, 31-33, 39) and Cl^- efflux (16, 40) (two important regulators of secretin-stimulated choleresis) (11, 16, 26, 28, 30-33, 40) in small and large cholangiocytes from normal and 7-day BDL mice. Following purification, small and large mouse cholangiocytes were incubated at 37°C for 1 hour to regenerate membrane proteins damaged by trypsin digestion during cell isolation (36). Subsequently, small and large cholangiocytes (1×10^5 cells) were stimulated at room temperature (7, 15, 16, 26, 31, 32, 39) with 0.2% bovine serum albumin (BSA, basal) or secretin (100 nM) (7, 15, 16) for 5 minutes (7, 15, 16, 26, 31, 32, 39) with 0.2% BSA. Following stimulation with secretin, 3-isobutylmethylxanthine, a phosphodiesterase inhibitor (41), which prevents cAMP degradation (7, 15, 16), was added to small and large cell suspension before ethanol extraction. RIA analysis (7, 15, 16) was performed in accordance with the instructions from the vendor.

Cl^- Efflux Studies—Cl^- efflux was evaluated in freshly isolated small and large cholangiocytes as described (42). The fluorescent probe N-(ethoxycarbonylmethyl)-6-methoxyquinolinium bromide (MQAE) and 4,4′-diisothiocyanatodihydrostilbene-2,2′-disulfonic acid disodium salt hydrate (H_2DIDS, competitive inhibitor of chloride exchange that does not cross the membrane) (43) were obtained from Invitrogen (Carlsbad, CA). Standard Ringer's solution consisted of: 140 mM NaCl, 5 mM KCl, 5 mM (2-hydroxyethyl)-N-piperazine N-2 ethanesulphonic acid (HEPES), 1 mM $MgCl_2$ and 5 mM glucose, pH 7.4. In chloride-free Standard Ringer's solution the chloride salts were exchanged for nitrate salts. K^+-rich calibration buffers were made by mixing of 150 nM chloride solution (120 mM KCl, 1 mM $MgCl_2$, 27 mM NaCl, 5 mM glucose and 5 mM HEPES), and 150 mM NO^-_3 solutions (chloride exchanged for nitrate) to obtain the desired concentrations of chloride. Briefly, freshly isolated small and large mouse cholangiocytes were loaded with 10 mM MQAE for 1 hour, rinsed in Standard Ringer's solution, and

allowed to attach to glass cover slips coated with BD Cell-Tak (BD Bioscience, Bedford, MA). Cover slips were placed in a chamber on the stage of an inverted microscope Nikon Eclipse TE300 (Nikon, Tokyo, Japan). Excitation light was at 355 nm and emission was measured at 460 nm using a CCD camera. Centers were bathed in Standard Ringer's solution. Images were captured for 16 ms every 3-8 seconds. The basal Cl^- efflux was measured during the exposure of the cells loaded with MQAE to a chloride gradient as described elsewhere(42). The fluorescence was expressed as relative change (F_{rel}) in fluorescence (F) to the initial fluorescence at the beginning of the experiment (F_o) according to: $F_{rel}=F/F_o \times 100$ (%). The relative chloride efflux rat (J_{Cl}) was determined from the first derivative of F_{rel} with time ($\Delta F_{rel}/\Delta t$), percent/s. The efflux via CFTR was determined by subtracting the basal relative efflux (J_{basal}) from the cAMP-stimulated relative rate (J_{cAMP}), according to: $J_{CFTR}=J_{cAMP}-J_{basal}$. For each experiment, 4 to 6 cells were analyzed and the average response was counted as one experimental data point. GraphPad Prism 5.0 software (GraphPad Software, San Diego, CA) was used to determine the value of the Cl^- efflux rate.

RESULTS

In Situ Morphometric Analysis of Intrahepatic Bile Ducts of Normal and BDL Mice

Normal mouse liver sections showed a significant difference in bile duct morphology and size (Figure 1, panels a and c) with cells lining the large ducts appearing to be more columnar compared to small ducts (Figure 1, panels b and d). In 3-day BDL mice, the liver sections also demonstrated a significant difference in bile duct morphology and size (not shown) with cells lining the large ducts appearing to be more columnar compared to small ducts, similar to that observed in normal mice liver sections (Figure 1, panels b and d). In addition, histological examination of liver sections from 3-day BDL mice revealed dilatation of small peripheral ducts (Figure 2 a and b), and as expected hepatocyte necrosis and ductal proliferation were also evident (Figure 2 c). Small and large bile duct areas of normal and 3-day BDL mice were significantly different from each other (Kruskal-Wallis One Way ANOVA on Ranks, $p<0.0001$) (Figure 3 a). The areas of cholangiocytes lining small and large bile ducts were also found to be significantly different (Kruskal-Wallis One Way ANOVA on Ranks, $p<0.0001$) (Figure 3 b). The areas (pixel count) of cholangiocytes lining small and large bile ducts significantly correlated with bile duct size (Figure 3 b), demonstrating that small cholangiocytes line small ducts and larger cholangiocytes line larger ducts.

Cell Size Distribution in Isolated Pooled and Small and Large Cholangiocytes from Normal and BDL Mice

Cell size distribution was determined in freshly isolated pooled and small and large cholangiocytes from normal, and 3- and 7-day BDL mice. The purity of the cells following immunomagnetic isolation was 99-100% as expected. Vimentin and G-6-P staining for contamination were negative (not shown). Cell size distribution for pooled cholangiocytes is illustrated in Figure 5. A shift in median values of cell size is visible from normal through 7 days of BDL to large cells based upon median cell size (Figure 4). There was a significant difference in the median cell size as determined by ANOVA (Kruskal-Wallis One Way ANOVA, $p<0.0006$. There were no variations in the pooled cell size distribution of mouse

cholangiocytes compared to rat cholangiocytes (7, 16). Mean cell size (μm) for freshly isolated small and large cholangiocytes from normal, 3-and 7-day BDL mice is presented in Table 1. As expected, there was a significant difference in the mean cell size of small and large cholangiocytes isolated from each treatment groups ($p<0.05$ large vs corresponding small) (Table 1).

BDL Stimulates the Proliferation of Large but not Small Mouse Bile Ducts and Isolated Cholangiocytes

Small and large bile duct mass expressed as a percentage, was evaluated by morphometry of KRT19 stained liver sections. The bile duct mass of large bile ducts was significantly increased in 3- and 7-day BDL mice sections (Figure 5 b and c) compared to normal sections (Figure 5 a). There were no significant variations in small bile duct mass across the three treatment groups (Figure 5). Cell cycle distributions of small and large cholangiocytes isolated from normal, and 3- and 7-day BDL mice were determined using FACS analysis (Table 2). There was a marked increase in the number of large cholangiocytes isolated from 3- and 7-day BDL mice in G2/M and S phase as compared to normal large cholangiocytes (Table 2). There were no significant changes in the cell cycle of small cholangiocytes isolated from the three treatment groups (Table 2).

Expression of SR, CFTR, Cl^-/HCO^-_3 AE2 and KRT19 in Liver Sections and Purified Small and Large Cholangiocytes

The expression of SR, CFTR, and Cl^-/HCO^-_3 AE2 was measured in liver sections from normal, 3-day and 7-day BDL mice by immunohistochemistry (Figure 6 and Table 3). SR, Cl^-/HCO^-_3 AE2 and CFTR are expressed by larger bile ducts (Figure 6 and Table 3), whereas small bile ducts are negative (not shown). Following BDL for 3 and 7 days, the expression of SR, Cl^-/HCO^-_3 AE2 and CFTR increased in larger bile ducts compared to large ducts of normal liver sections (Figure 7 and Table 3); in small bile ducts staining for SR, Cl^-/HCO^-_3 AE2, and CFTR remained negative (not shown). As expected (44), CFTR expression is largely apical in nature (Figure 6). When liver sections were incubated with pre-immune serum substituted for the primary antibody the staining was absent (not shown). The semiquantitative expression of SR, Cl^-/HCO^-_3 AE2, and CFTR in small and large ducts in sections from normal, 3- and 7-day BDL mice is shown in Table 3.

The expression of SR, CFTR, and Cl^-/HCO^-_3 AE2 was also evaluated by immunofluorescence in freshly isolated small and large cholangiocytes from normal, and 3- and 7-day BDL mice (Figure 7). Both small and large cholangiocytes expressed KRT19 (Figure 7). Parallel with the immunohistochemistry (Figure 6), large (but not small) cholangiocytes were positive for SR, CFTR, and Cl^-/HCO^-_3 AE2 (Figure 7).

Effect of Secretin on Intracellular cAMP Levels and Cl^- Efflux in Small and Large Normal Mouse Cholangiocytes

Similar to what was observed in the rat biliary epithelium (7, 14, 16), secretin increased cAMP levels in large (but not small) cholangiocytes isolated from normal, and 7-day BDL mice, compared to large cholangiocytes treated with 0.2% BSA (basal) (Figure 8 a). The increase in secretin-stimulated cAMP levels (observed after BDL for 7 days) was higher

compared to normal large cholangiocytes (Figure 8 a). Similarly, secretin increased Cl^- efflux in large cholangiocytes from normal and 7-day BDL mice (Figure 9 b). The increase in Cl^- efflux observed in large cholangiocytes was higher in 7-day BDL compared to normal large cholangiocytes (Figure 8 b).

Discussion

The morphological and functional heterogeneity of cholangiocytes in rats has been defined during the past years (1, 7, 10, 14-16, 18, 45). Whether a similar morphologic, proliferative and functional profile exists in mice is relatively unknown (19). We have developed a SV-40 transformed small and large cholangiocyte cell line from mice (46), which have morphological, phenotypic and functional characteristics similar to that of freshly isolated rat (7, 16) and mouse (19) small and large cholangiocytes. However, cholangiocyte heterogeneity has not been explored *in situ* (in liver sections) and freshly isolated small and large mouse cholangiocytes and liver sections from normal and BDL (3 and 7 days post-surgery) mice. We believe that our data on mouse cholangiocyte heterogeneity is critical due to the increased usage of knockout mouse models to study cholestatic liver diseases, such as mdr2 and CGRP knockout mice (35, 47).

The morphological and functional diversity of epithelial cells in other organs including kidney (48, 49), the small intestine (50, 51), and parenchyma liver (52, 53) and the rat biliary epithelium (1, 5, 7, 10, 13-18) is well defined. Indeed, only the epithelial cells of the proximal tubule and descending limb of Henle's loop have trans-epithelial water secretory activity modulated by aquaporin channels (CHIP28) (54). The epithelial cells of the small and large intestine are heterogeneous regarding the distribution of the membrane transporters regulating the absorptive and secretory functions (50). In the liver, periportal and perivenous parenchymal cells are heterogeneous regarding the metabolism of oxidative energy, carbohydrate and amino acids (52). Furthermore, the expression of transporters regulating bile secretion is heterogeneous among hepatocytes of different lobular zones (53). Although, the heterogeneity of the rat biliary epithelium is well established, limited information exists (19) regarding the possible functional diversity of different sized mouse cholangiocytes.

We first demonstrated that the biliary epithelium of normal mice is morphologically heterogeneous with smaller cholangiocytes lining small bile ducts and larger cholangiocytes lining larger ducts. The latter data is important since it allows the direct correlation of studies on purified subpopulations of small and large cholangiocytes to specific bile duct segments in the intrahepatic mouse biliary tree. Our present findings parallel closely what has been demonstrated in the rat ductal biliary system. Indeed, we have shown that the rat biliary tree is composed of bile ducts of different sizes (small ducts lined by small cells and larger ducts lined by larger cholangiocytes), which range in size from 5 to 200 μm in external diameter (7). Based upon morphological, phenotypic and functional differences among ducts of different diameter in a rat model, we have recently classified the intrahepatic bile duct system into small (< 15 μm) and large (> 15 μm) ducts (14). Similar results were obtained in normal rats by Benedetti et al. (8), who demonstrated that: (i) the diameter of intrahepatic bile ducts ranges from 5 to 100 μm, and the area of lining cholangiocytes ranges

from 8 to 100 μm; and (ii) a highly significant linear relationship existed between duct diameter and cholangiocytediameter. During the model of cholestasis induced by BDL, there were similar differences in bile duct morphology, which was consistent with what was observed in normal mice. As expected, histological examination of BDL mice liver sections also revealed hepatocyte necrosis and the dilation of small peripheral bile ducts (15, 16). In 3-day BDL mice, the size of the cholangiocytes correlated to bile ducts diameter *in situ*, with small cholangiocytes lining small bile ducts and larger cholangiocytes lining larger bile ducts.

We have previously demonstrated that BDL induces the proliferation of large but not small rat cholangiocytes (16, 18). Consistent with those findings (16, 18), we found, byKRT19 morphometry for small and large ducts in liver sections and by FACS analysis of the cell cycle of small and large cholangiocytes isolated from normal and 3- and 7-day mice that there was selective proliferation of large but not small mouse cholangiocytes. These findings clearly demonstrate that cholangiocytes from mice have the same proliferative heterogeneity profile as rats supporting the use of the mouse model of BDL for studies elucidating the proliferative responses of small and large cholangiocytes to extrahepatic cholestasis.

Next, we evaluated the heterogeneous expression of functional markers of cholangiocytes, such as SR, CTFR and Cl^-/HCO^-_3, which are involved in the regulation of cholangiocyte secretory and proliferative activities (1, 5, 7, 10, 13-18). Previous work has shown that large cholangiocytes from rats are functionally active (i.e., respond to secretin) and express SR, CFTR and the Cl^-/HCO^-_3 exchanger (5, 7, 13, 14, 16). Similar to rats (5, 7, 13, 14, 16) we found that large but not small cholangiocytes and bile ducts express SR, CFTR and Cl^-/HCO^-_3 exchanger indicating that large cholangiocyte from mice are functionally active, cAMP responsive and heterogeneous in response to cholestasis induced by BDL. The heterogeneous secretory and proliferative activities of the mouse biliary epithelium were further supported by the enhanced cAMP levels and Cl^- efflux (in response to secretin) in large but not small cholangiocytes from normal and BDL mice. The pathophysiology of small cholangiocytes is largely unknown. To compensate for the loss of large, cAMP-dependent cholangiocyte function, small rat cholangiocytes have been shown to proliferate and develop *de novo* SR gene expression and secretin-stimulated secretory activity (10, 18). Our recent studies (19) demonstrated that small murine cholangiocytes proliferate by activation (in response to H1 histamine receptor agonists) of the IP_3/CaMK I/CREB pathway (19), which is independent from the cAMP-dependent pathway shown in large cholangiocytes (5, 7, 13-16).

In conclusion, we have demonstrated that small and large bile ducts and small and large cholangiocytes from normal and BDL mice display morphologic, proliferative and functional heterogeneity. Our present findings demonstrated that the biliary system in mice has morphologic, proliferative and secretory heterogeneity similar to the normal and BDL rat models (5, 7, 8, 13-16), thereby supporting the usage of genetically modified mouse models in the study of biliary heterogeneity and cholestatic liver diseases. This information on the heterogeneity of biliary epithelium in the mouse will be valuable for future studies examining cholestatic liver disease pathogenesis. In particular, factors and signaling mechanisms controlling the heterogeneous responses of small and large cholangiocytes

during cholestatic liver diseases and exposure to liver toxins can be addressed in specific transgenic mouse models for key proteins thought to play a role in biliary proliferation.

Acknowledgments

We thank Dr. Andreea Trache and Anna Webb of the Texas A&M University Health Science Center Microscopy Imaging Center for assistance with confocal microscopy.

This work was supported by the Dr. Nicholas C. Hightower Centennial Chair of Gastroenterology to Dr. Alpini from Scott & White, a VA Research Scholar Award, a VA Merit Award and the NIH grants DK054811 and DK062975 to Dr. Alpini, by a grant from MIUR (PRIN) 2007 #2007HPT7BA_001), University and Faculty funds (Prof. Eugenio Gaudio), by MIUR (PRIN) grants: #2007, prot. HPT7BA_003 to Prof. Alvaro and an NIH K01 grant award (DK078532) to Dr. DeMorrow.

Abbreviations used

BDL	bile duct ligation
BDI	bile duct incannulation
BSA	bovine serum albumin
cAMP	cyclic adenosine 3′, 5′-monophosphate
Cl^-/HCO^-_3AE2	chloride bicarbonate anion exchanger 2
CCl_4	carbon tetrachloride
CFTR	cystic fibrosis transmembrane conductance regulator
KRT19	keratin 19
DAPI	dye 4,6-diamidino-2-phenylindole
FACS	fluorescence activated cell sorting
H&E	hematoxylin and eosin
PBC	primary biliary cirrhosis
PBS	phosphate buffered saline
PSC	primary sclerosing cholangitis
SR	secretin receptor

REFERENCES

1. Alpini, G.; Prall, RT.; LaRusso, NF. The pathobiology of biliary epithelia. In: Arias, IM.; Boyer, JL.; Chisari, FV.; Fausto, N.; Jakoby, W.; Schachter, D.; Shafritz, DDA., editors. The Liver; Biology & Pathobiology. 4. Lippincott Williams & Wilkins; Philadelphia, PA: 2001. p. 421-435.
2. Alvaro D, Mancino MG, Glaser S, Gaudio E, Marzioni M, Francis H, et al. Proliferating cholangiocytes: a neuroendocrine compartment in the diseased liver. Gastroenterology. 2007; 132:415–431. [PubMed: 17241889]
3. Lazaridis KN, Strazzabosco M, LaRusso NF. The cholangiopathies: disorders of biliary epithelia. Gastroenterology. 2004; 127:1565–1577. [PubMed: 15521023]
4. Alpini G, Lenzi R, Sarkozi L, Tavoloni N. Biliary physiology in rats with bile ductular cell hyperplasia. Evidence for a secretory function of proliferated bile ductules. J Clin Invest. 1988; 81:569–578. [PubMed: 2448343]

5. Kanno N, LeSage G, Glaser S, Alvaro D, Alpini G. Functional heterogeneity of the intrahepatic biliary epithelium. Hepatology. 2000; 31:555–561. [PubMed: 10706542]
6. Ludwig J. New concepts in biliary cirrhosis. Sem Liver Dis. 1987; 7:293–301.
7. Alpini G, Roberts S, Kuntz SM, Ueno Y, Gubba S, Podila PV, et al. Morphological, molecular, and functional heterogeneity of cholangiocytes from normal rat liver. Gastroenterology. 1996; 110:1636–1643. [PubMed: 8613073]
8. Benedetti A, Bassotti C, Rapino K, Marucci L, Jezequel AM. A morphometric study of the epithelium lining the rat intrahepatic biliary tree. J Hepatol. 1996; 24:335–342. [PubMed: 8778202]
9. Schaffner F, Popper H. Electron microscopic studies of normal and proliferated bile ductules. Am J Pathol. 1961; 38:393–410. [PubMed: 13747220]
10. LeSage G, Benedetti A, Glaser S, Marucci L, Tretjak Z, Caligiuri A, et al. Acute carbon tetrachloride feeding selectively damages large, but not small, cholangiocytes from normal rat liver. Hepatology. 1999; 29:307–319. [PubMed: 9918904]
11. Kanno N, LeSage G, Glaser S, Alpini G. Regulation of cholangiocyte bicarbonate secretion. Am J Physiol Gastrointest Liver Physiol. 2001; 281:G612–625. [PubMed: 11518673]
12. Neil DA, Hubscher SG. Histologic and biochemical changes during the evolution of chronic rejection of liver allografts. Hepatology. 2002; 35:639–651. [PubMed: 11870379]
13. Marzioni M, Glaser SS, Francis H, Phinizy JL, LeSage G, Alpini G. Functional heterogeneity of cholangiocytes. Semin Liver Dis. 2002; 22:227–240. [PubMed: 12360417]
14. Alpini G, Glaser S, Robertson W, Rodgers RE, Phinizy JL, Lasater J, et al. Large but not small intrahepatic bile ducts are involved in secretin-regulated ductal bile secretion. Am J Physiol Gastroint Liver Physiol. 1997; 272:G1064–1074.
15. Alpini G, Glaser S, Ueno Y, Pham L, Podila PV, Caligiuri A, et al. Heterogeneity of the proliferative capacity of rat cholangiocytes after bile duct ligation. Am J Physiol Gastrointest Liver Physiol. 1998; 274:G767–775.
16. Alpini G, Ulrich C, Roberts S, Phillips JO, Ueno Y, Podila PV, et al. Molecular and functional heterogeneity of cholangiocytes from rat liver after bile duct ligation. Am J Physiol Gastrointest Liver Physiol. 1997; 272:G289–297.
17. LeSage G, Glaser S, Ueno Y, Alvaro D, Baiocchi L, Kanno N, et al. Regression of cholangiocyte proliferation after cessation of ANIT feeding is coupled with increased apoptosis. Am J Physiol Gastrointest Liver Physiol. 2001; 281:G182–190. [PubMed: 11408271]
18. LeSage G, Glaser SS, Marucci L, Benedetti A, Phinizy JL, Rodgers R, et al. Acute carbon tetrachloride feeding induces damage of large but not small cholangiocytes from BDL rat liver. Am J Physiol Gastrointest Liver Physiol. 1999; 276:G1289–1301.
19. Francis H, Glaser S, DeMorrow S, Gaudio E, Ueno Y, Venter J, et al. Small mouse cholangiocytes proliferate in response to H1 histamine receptor stimulation by activation of the IP_3/CaMK I/CREB pathway. Am J Physiol Cell Physiol. 2008; 295:C499–513. [PubMed: 18508907]
20. Steiner JW, Carruthers JS. Studies on the fine structure of the terminal branches of the biliary tree. I. The morphology of normal bile canaliculi, bile preductules (ducts of Hering) and bile ductules. Am J Pathol. 1961; 38:639–661. [PubMed: 19971000]
21. Nathanson MH, Boyer JL. Mechanisms and regulation of bile secretion. Hepatology. 1991; 14:551–566. [PubMed: 1874500]
22. Alpini G, Glaser S, Robertson W, Phinizy JL, Rodgers RE, Caligiuri A, et al. Bile acids stimulate proliferative and secretory events in large but not small cholangiocytes. Am J Physiol Gastroint Liver Physiol. 1997; 273:G518–529.
23. Alpini G, Lenzi R, Zhai W-R, Slott PA, Liu MH, Sarkozi L, et al. Bile secretory function of intrahepatic biliary epithelium in the rat. Am J Physiol Gastroint Liver Physiol. 1989; 257:G124–G133.
24. Alvaro D, Cho WKC, Mennone A, Boyer JL. Effect of secretin on intracellular pH regulation in isolated rat bile duct epithelial cells. J Clin Invest. 1993; 92:1314–1325. [PubMed: 8397224]
25. Alvaro D, Alpini G, Jezequel AM, Bassotti C, Francia C, Fraioli F, et al. Role and mechanisms of action of acetylcholine in the regulation of rat cholangiocyte secretory functions. J Clin Invest. 1997; 100:1349–1362. [PubMed: 9294100]

26. Glaser S, Rodgers RE, Phinizy JL, Robertson WE, Lasater J, Caligiuri A, et al. Gastrin inhibits secretin-induced ductal secretion by interaction with specific receptors on rat cholangiocytes. Am J Physiol Gastrointest Liver Physiol. 1997; 273:G1061–1070.
27. Glaser S, Alvaro D, Roskams T, Phinizy JL, Stoica G, Francis H, et al. Dopaminergic inhibition of secretin-stimulated choleresis by increased PKC-γ expression and decrease of PKA activity. Am J Physiol Gastrointest Liver Physiol. 2003; 284:G683–G694. [PubMed: 12505882]
28. LeSage G, Alvaro D, Benedetti A, Glaser S, Marucci L, Baiocchi L, et al. Cholinergic system modulates growth, apoptosis, and secretion of cholangiocytes from bile duct-ligated rats. Gastroenterology. 1999; 117:191–199. [PubMed: 10381927]
29. LeSage G, Alvaro D, Glaser S, Francis H, Marucci L, Roskams T, et al. Alpha-1 adrenergic receptor agonists potentiate secretin-stimulated choleresis of bile duct ligated rats by Ca^{2+}- and PKC-dependent stimulation of cAMP synthesis. Hepatology. 2004; 40:1116–1127. [PubMed: 15486932]
30. LeSage G, Marucci L, Alvaro D, Glaser SS, Benedetti A, Marzioni M, et al. Insulin inhibits secretin-induced ductal secretion by activation of PKC alpha and inhibition of PKA activity. Hepatology. 2002; 36:641–651. [PubMed: 12198656]
31. LeSage G, Glaser S, Gubba S, Robertson WE, Phinizy JL, Lasater J, et al. Regrowth of the rat biliary tree after 70% partial hepatectomy is coupled to increased secretin-induced ductal bile secretion. Gastroenterology. 1996; 111:1633–1644. [PubMed: 8942744]
32. Glaser S, Benedetti A, Marucci L, Alvaro D, Baiocchi L, Kanno N, et al. Gastrin inhibits cholangiocyte growth in bile duct-ligated rats by interaction with cholecystokinin-B/Gastrin receptors via D-myo-inositol 1,4,5-triphosphate-, $Ca(^{2+})$-, and protein kinase C alpha-dependent mechanisms. Hepatology. 2000; 32:17–25. [PubMed: 10869284]
33. Tietz PS, Alpini G, Pham LD, LaRusso NF. Somatostatin inhibits secretin-induced ductal hypercholeresis and exocytosis by cholangiocytes. Am J Physiol Gastrointest Liver Physiol. 1995; 269:G110–118.
34. Miyoshi H, Rust C, Guicciardi ME, Gores GJ. NF-kappaB is activated in cholestasis and functions to reduce liver injury. Am J Pathol. 2001; 158:967–975. [PubMed: 11238044]
35. Glaser S, Ueno Y, DeMorrow S, Chiasson VL, Katki KA, Venter J, et al. Knockout of alpha-calcitonin gene-related peptide reduces cholangiocyte proliferation in bile duct ligated mice. Lab Invest. 2007; 87:914–926. [PubMed: 17618297]
36. Ishii M, Vroman B, LaRusso NF. Isolation and morphological characterization of bile duct epithelial cells from normal rat liver. Gastroenterology. 1989; 97:1236–1247. [PubMed: 2792660]
37. Teutsch HF. Improved method for the histochemical demonstration of glucose-6-phosphatase activity. Histochemistry. 1978; 57(2):107–117. [PubMed: 211104]
38. Kalejta RF, Shenk T, Beavis AJ. Use of a membrane-localized green fluorescent protein allows simultaneous identification of transfected cells and cell cycle analysis by flow cytometry. Cytometry. 1997; 29:286–291. [PubMed: 9415410]
39. Kato A, Gores GJ, LaRusso NF. Secretin stimulates exocytosis in isolated bile duct epithelial cells by a Cyclic AMP-mediated mechanism. J Biol Chem. 1992; 267:15523–15529. [PubMed: 1322400]
40. McGill JM, Basavappa S, Gettys TW, Fitz JG. Secretin activates Cl^-channels in bile duct epithelial cells through a cAMP-dependent mechanism. Am J Physiol Gastroint Liver Physiol. 1994; 266:G731–736.
41. Rapundalo ST, Solaro RJ, Kranias EG. Inotropic responses to isoproterenol and phosphodiesterase inhibitors in intact guinea pig hearts: comparison of cyclic AMP levels and phosphorylation of sarcoplasmic reticulum and myofibrillar proteins. Circ Res. 1989; 64:104–111. [PubMed: 2535795]
42. Servetnyk Z, Krjukova J, Gaston B, Zaman K, Hjelte L, Roomans GM, et al. Activation of chloride transport in CF airway epithelial cell lines and primary CF nasal epithelial cells by S-nitrosoglutathione. Respir Res. 2006; 7:124. [PubMed: 17022806]
43. Furuya W, Tarshis T, Law FY, Knauf PA. Transmembrane effects of intracellular chloride on the inhibitory potency of extracellular H2DIDS. Evidence for two conformations of the transport site

of the human erythrocyte anion exchange protein. J Gen Physiol. 1984; 83:657–681. [PubMed: 6736915]

44. Fiorotto R, Spirli C, Fabris L, Cadamuro M, Okolicsanyi L, Strazzabosco M. Ursodeoxycholic acid stimulates cholangiocyte fluid secretion in mice via CFTR-dependent ATP secretion. Gastroenterology. 2007; 133:1603–1613. [PubMed: 17983806]
45. Alpini G, Glaser S, Ueno Y, Rodgers R, Phinizy JL, Francis H, et al. Bile acid feeding induces cholangiocyte proliferation and secretion: evidence for bile acid-regulated ductal secretion. Gastroenterology. 1999; 116:179–186. [PubMed: 9869616]
46. Ueno Y, Alpini G, Yahagi K, Kanno N, Moritoki Y, Fukushima K, et al. Evaluation of differential gene expression by microarray analysis in small and large cholangiocytes isolated from normal mice. Liver Int. 2003; 23:449–459. [PubMed: 14986819]
47. Trauner M, Fickert P, Wagner M. MDR3 (ABCB4) defects: a paradigm for the genetics of adult cholestatic syndromes. Semin Liver Dis. 2007; 27:77–98. [PubMed: 17295178]
48. Tsuruoka S, Takeda M, Yoshitomi K, Imai M. Cellular heterogeneity of ammonium ion transport across the basolateral membrane of the hamster medullary thick ascending limb of Henle's loop. J Clin Invest. 1993; 92:1881–1888. [PubMed: 8408639]
49. Guggino WB. Functional heterogeneity in the early distal tubule of the Amphiuma kidney: evidence for two modes of Cl^- and K^+ transport across the basolateral cell membrane. Am J Physiol Renal Physiol. 1986; 250:F430–440.
50. Knickelbein RG, Aronson PS, Dobbins JW. Membrane distribution of sodium-hydrogen and chloride-bicarbonate exchangers in crypt and villus cell membranes from rabbit ileum. J Clin Invest. 1988; 82:2158–2163. [PubMed: 2848868]
51. Fromm M, Hegel U. Segmental heterogeneity of epithelial transport in rat large intestine. Pflugers Arch. 1978; 378:71–83. [PubMed: 569827]
52. Katz, N.; Jungermann, K. Metabolic heterogeneity of the liver. In: Tavoloni; Berk, PD., editors. Hepatic transport and bile secretion: physiology and pathophysiology. New York; Raven Press: 1993. p. 55-70.
53. Groothuis GM, Meijer DK. Hepatocyte heterogeneity in bile formation and hepatobiliary transport of drugs. Enzyme. 1992; 46:94–138. [PubMed: 1289085]
54. Nielsen S, Smith BL, Christensen EI, Knepper MA, Agre P. CHIP28 water channels are localized in constitutively water-permeable segments of the nephron. J Cell Biol. 1993; 120:371–383. [PubMed: 7678419]

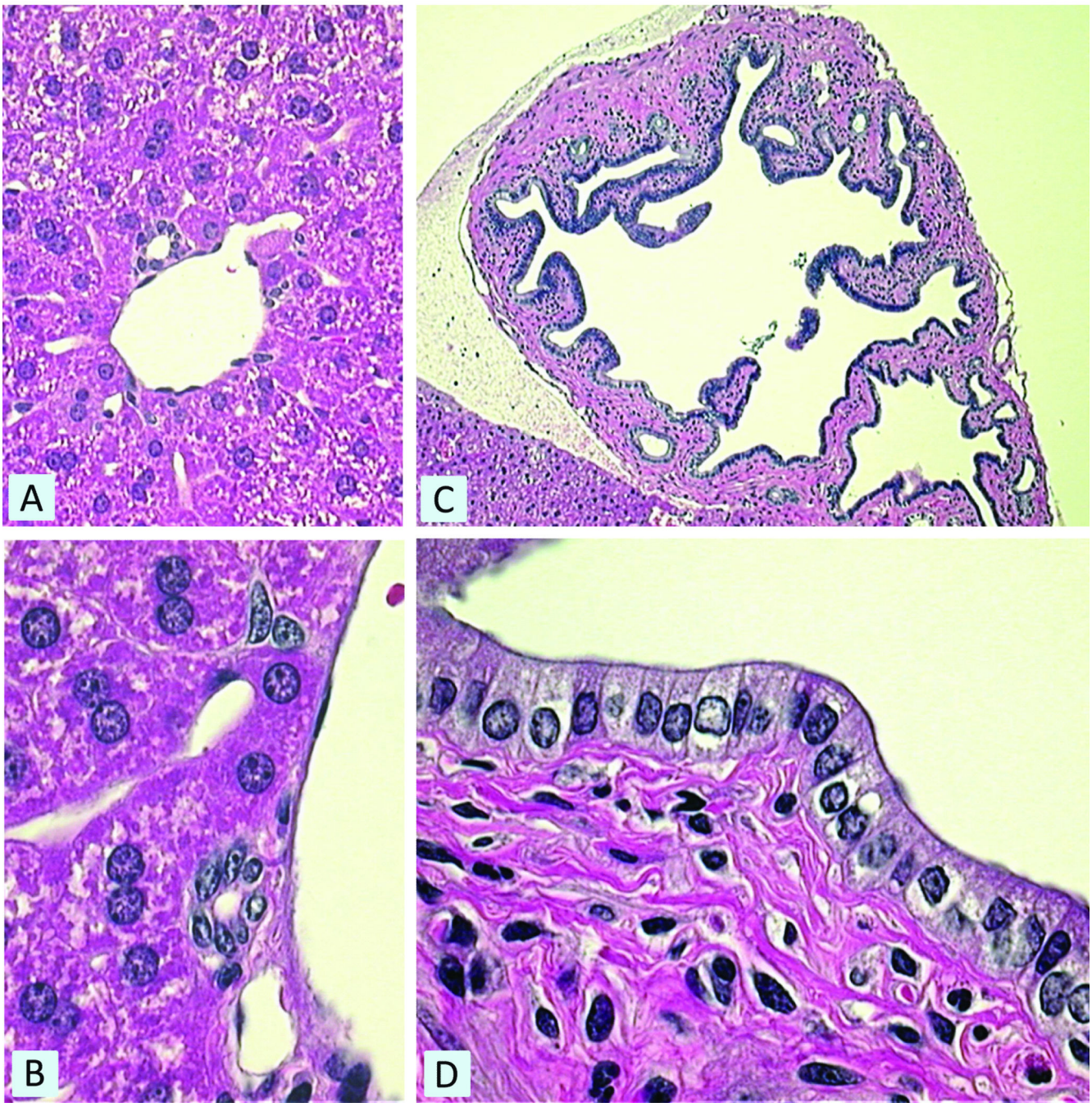

Figure 1.

In situ morphometric analysis of liver sections from normal mice. Morphometry of small bile ducts (panel A) and large bile ducts (panel C) illustrates the vast differences in bile duct structure and cholangiocyte morphology between small and large bile ducts. Cholangiocytes lining the large ducts (panel D) appear to be more columnar in morphology compared to small ducts (panel B). Magnification: (panel A) 400X, (panel B) 1000X, (panel C) 100X, and (panel D) large bile duct 1000X.

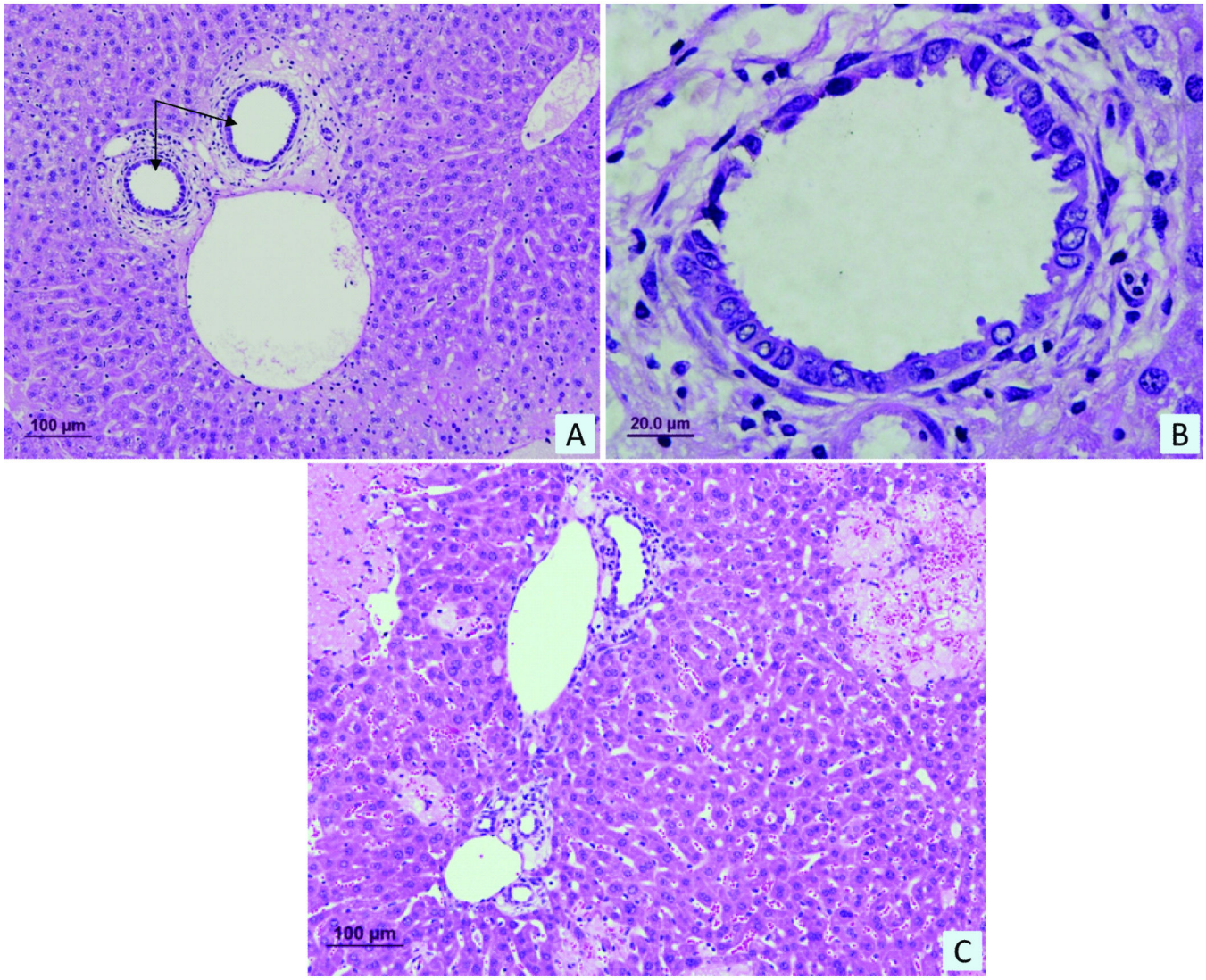

Figure 2.

(A) Histological examination of liver sections from 3-day BDL mice stained with H&E revealed dilation of small peripheral ducts indicated by black arrows. (B) Higher magnification view of dilated small peripheral ducts. (C) Hepatocyte necrosis and ductal proliferation were also evident in liver sections from 3-day BDL mice. Size in μm is indicated by black bar.

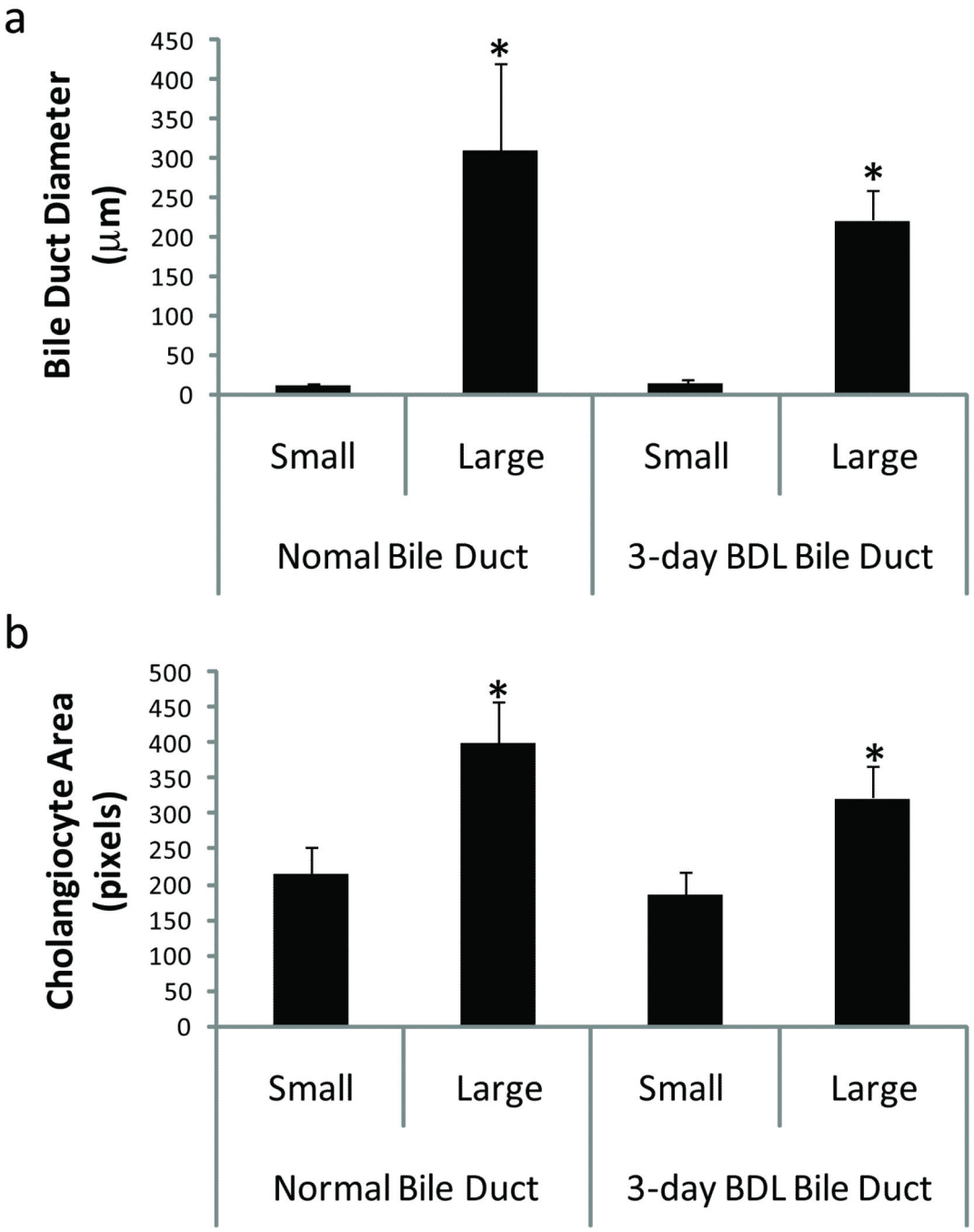

Figure 3.

In situ morphometric analysis of liver sections from normal and 3-day BDL mice. (A) Distribution of bile duct sizes (μm) classified as small and large bile ducts reveals a significant variation in bile duct size. (B) Distribution of cholangiocyte area (μm^2) lining small and large bile ducts indicates a correlation between cholangiocyte size and bile duct diameter. (Kruskal-Wallis One Way ANOVA on Ranks, *$p<0.0001$). BDL = bile duct ligation.

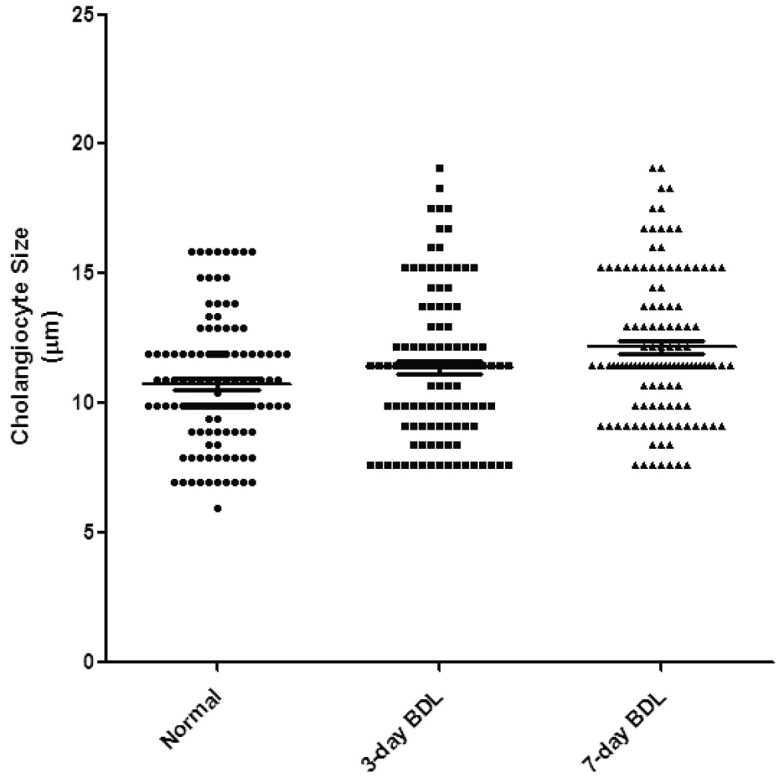

Figure 4.

Cell size distribution of freshly isolated pooled cholangiocytes from normal, 3- and 7-day BDL mice. The median size of cholangiocytes is increased in cholangiocytes from 3- and 7-day BDL mice compared to normal cholangiocytes. BDL = bile duct ligation.

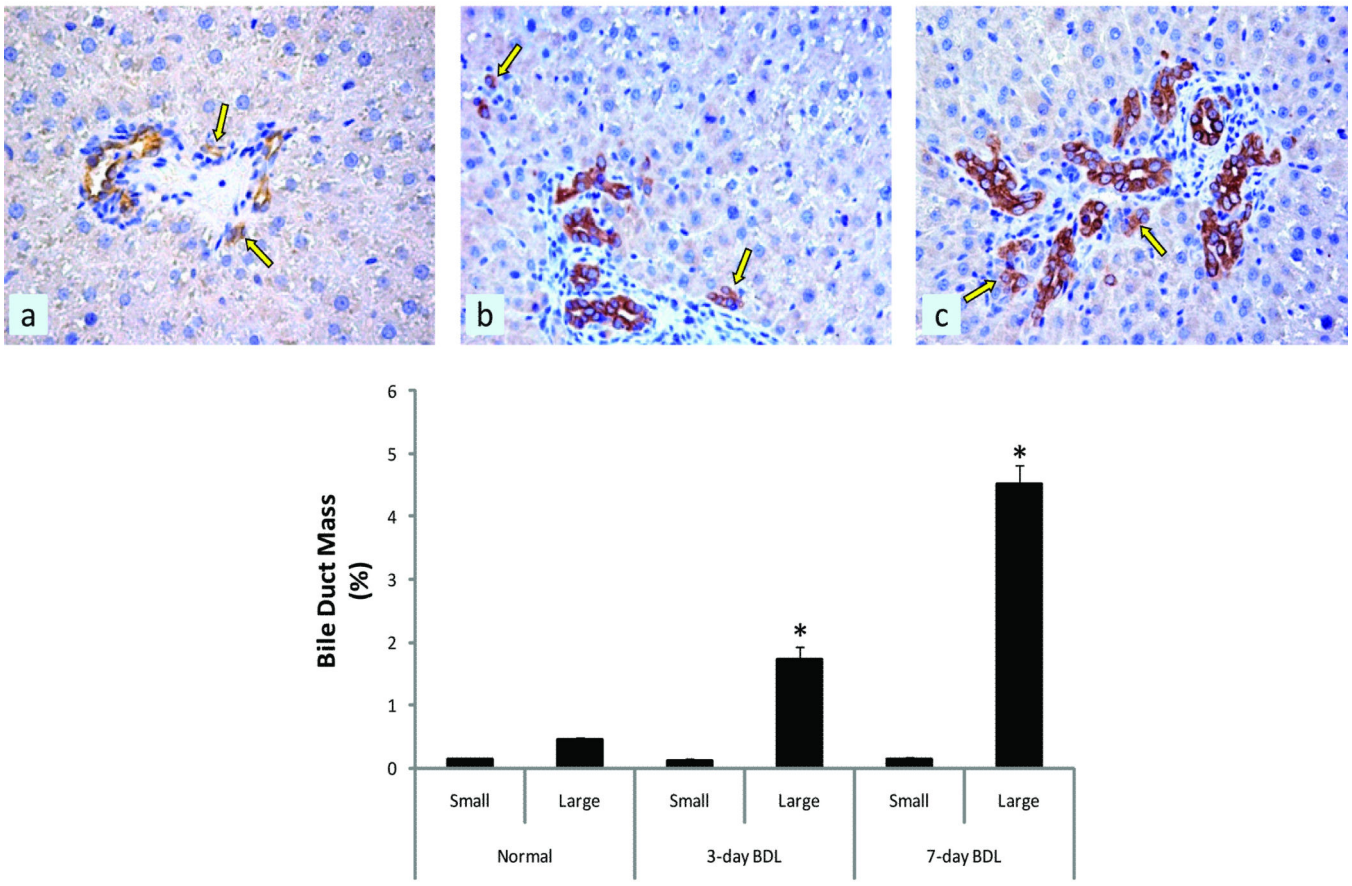

Figure 5.

Morphometric evaluation of small and large bile duct mass in liver sections stained with KRT19. There was a significant increase in large (but not small) bile duct mass in (B) 3-day and (C) 7-day BDL 7d mouse liver sections compared to (A) normal liver sections. (Bottom graph) Quantitative data of small and large bile duct mass evaluations. Data are expressed as mean ± SEM. BDL = bile duct ligation.

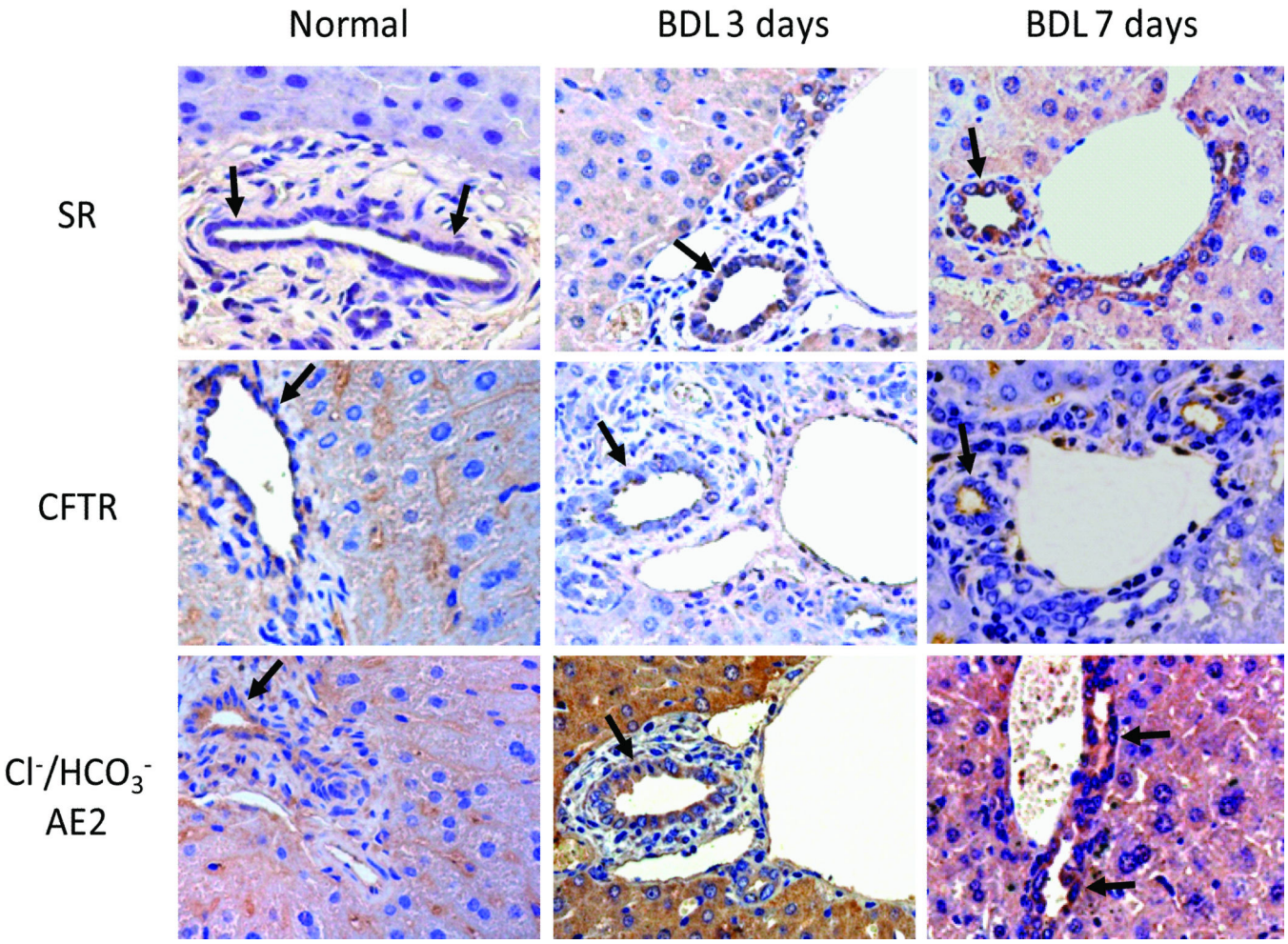

Figure 6.

Immunohistochemistry for SR, Cl^-/HCO^-_3 AE2, and CFTR in liver sections from normal, 3-day and 7-day BDL mice. SR, Cl^-/HCO^-_3 AE2 and CFTR are expressed by larger bile ducts, whereas small bile ducts are negative (not shown). Following BDL for 3 and 7 days, the expression of SR, Cl^-/HCO^-_3 AE2 and CFTR increases in larger bile ducts compared to large dusts of normal liver sections; in small bile ducts staining for SR, Cl^-/HCO^-_3 AE2, and CFTR remained negative (not shown). Arrows indicate large bile ducts. BDL = bile duct ligation; Cl^-/HCO^-_3 AE2 = chloride bicarbonate anion exchanger 2; CFTR = cystic fibrosis transmembrane conductance regulator; SR = secretin receptor.

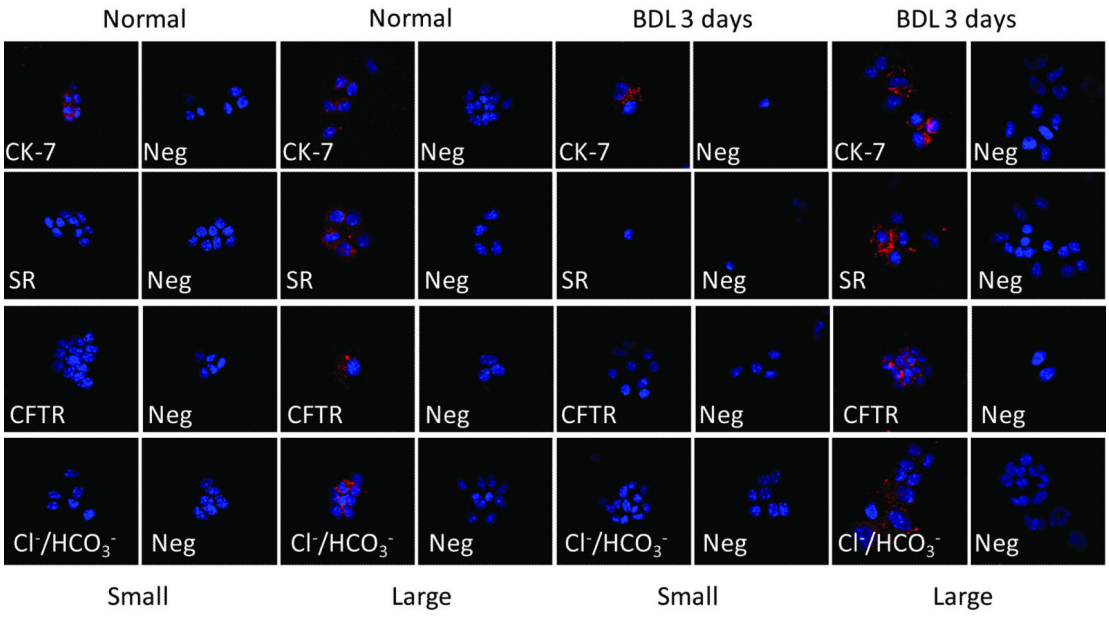

Figure 8 (panel b)

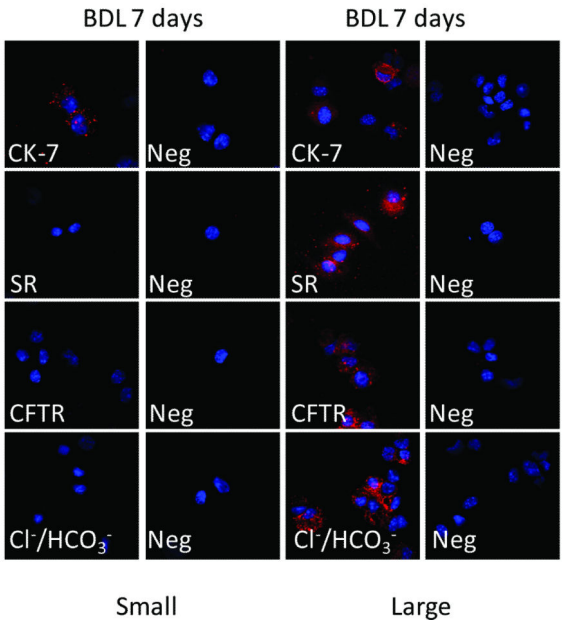

Figure 7.

Immunofluorescence for KRT19, SR, Cl^-/HCO^-_3 AE2 and CFTR expression in freshly isolated small and large cholangiocytes from [panel a] normal, 3- and [panel b] 7-day BDL mice. Both small and large cholangiocytes from normal, BDL 3d and BDL 7d mice express KRT19. Large (but not small) cholangiocytes from normal, 3- and 7-day BDL mice were positive for SR, CFTR, and Cl^-/HCO^-_3 AE2. Scale bar = 50 μm. BDL = bile duct ligation; KRT19 = keratin-19; Cl^-/HCO^-_3 = chloride bicarbonate anion exchanger 2; CFTR = cystic fibrosis transmembrane conductance regulator; SR = secretin receptor; Neg = negative.

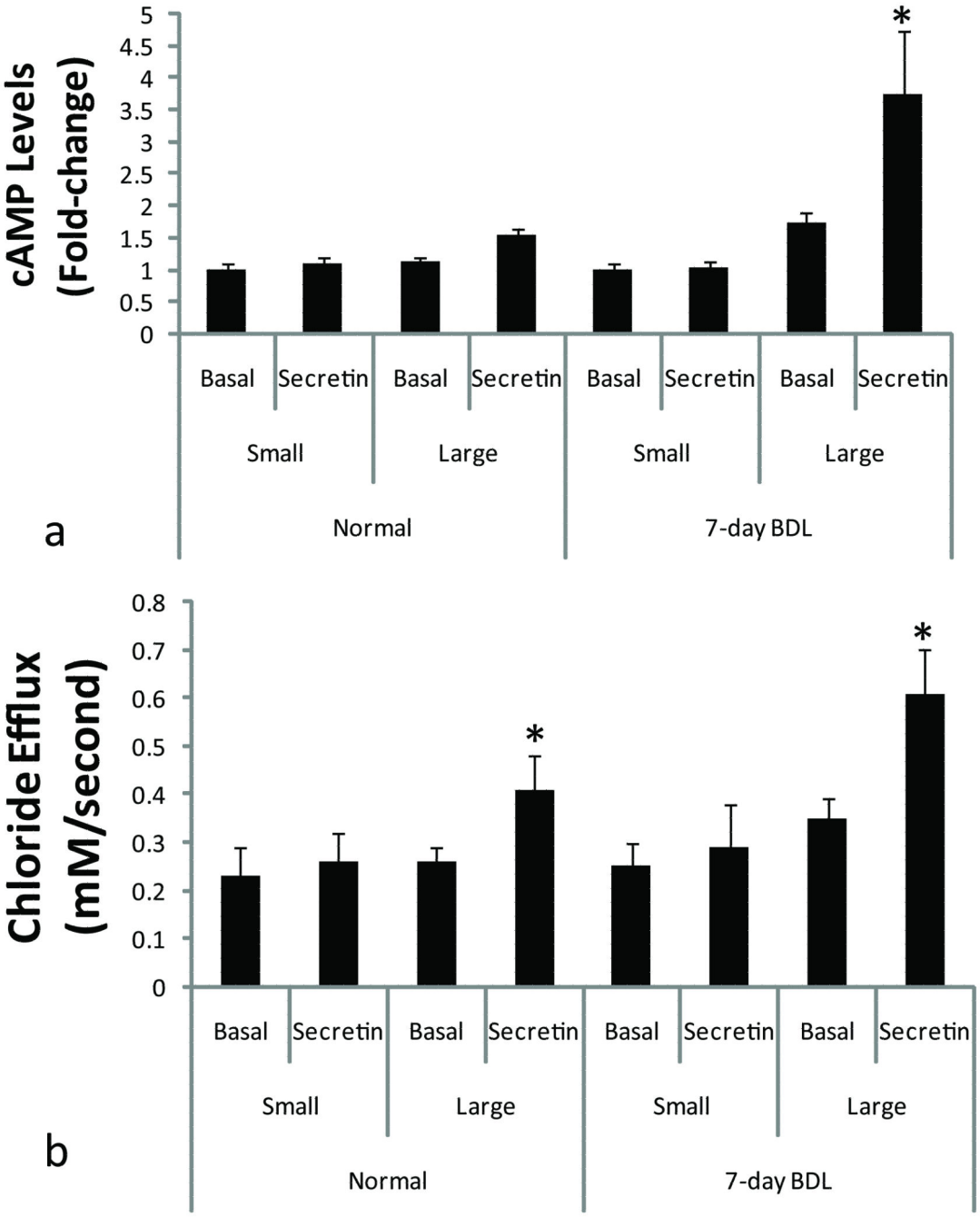

Figure 8.

Effects of secretin on [A] intracellular cAMP levels and [B] Cl^- efflux of small and large cholangiocytes. [A] Secretin (100 nM) increased cAMP levels in large (but not small) cholangiocytes isolated from normal and 7-day BDL mice compared to large cholangiocytes treated with 0.2% BSA (basal). Data are mean ± SEM of 8 experiments *$p<0.05$ vs. corresponding basal value. The increase in secretin-stimulated cAMP levels (observed after BDL for 7 days) was higher compared to normal large cholangiocytes. [B] Secretin (100 nM) increased Cl^- efflux of large (but not small) cholangiocytes isolated from normal and 7-

day BDL mice. Values are the mean ± SEM; n = 4 experiments for small cholangiocytes, and n = 6 experiments for large cholangiocytes for both normal and 7-day BDL. *p<0.05 vs. corresponding basal value.

Table 1

Mean cell sizes of small and large cholangiocytes isolated from normal, BDL 3- and 7-day BDL mice.

	Small	Large
Normal	8.84 ± 0.08	13.24 ± 0.17[&]
BDL 3d	7.98 ± 0.13	13.04 ± 0.20[&]
BDL 7d	8.02 ± 0.21	13.72 ± 0.27[&]

[&]$p<0.05$ large vs. corresponding small cholangiocytes. BDL = bile duct ligation.

Table 2

Cell cycle analysis of small and large cholangiocyte isolated from normal, and 3- and 7-day BDL mice.

		G1	G2	S
Normal	**Small**	99.57%	0.00%	0.43%
	Large	96.44%	0.00%	3.56%
BDL 3 days	**Small**	99.18%	0.12%	0.70%
	Large	86.60%	7.29%	6.11%
BDL 7 days	**Small**	98.19%	0.00%	1.81%
	Large	91.34%	3.35%	5.31%

The percentage of cells in Go/G1, S and G2/M phases of the cell cycle were determined using software analysis (Modfit LT 3.0). Analysis was performed on singlets, in which cell aggregates were eliminated by gating FL3-Width versus FL3-Area. BDL = bile duct ligation.

Table 3

Semiquantitative expression of SR, Cl^-/HCO^-_3 AE2 and CFTR in liver sections from normal, 3- and 7-day BDL mice.

	Normal		BDL		7 days BDL	
	Small	Large	Small	Large	Small	Large
SR	-	+	+/-	+++	+/-	+++
Cl^-/HCO^-_3AE2	-	++	+/-	+++	+/-	+++
CFTR	-	+	+/-	++	+/-	++

Parameters for the semi-quantitative evaluation of SR, Cl^-/HCO^-_3AE2 and CFTR in liver sections (5 mm thick; 3 slides evaluated per group of animals). CFTR = cystic fibrosis transmembrane conductance regulator. BDL = bile duct ligation; Cl^-/HCO^-_3AE2 = chloride bicarbonate anion exchanger 2; SR = secretin receptor. Grading: 0 – 5% = -; 6-10%= +/-; 11 – 30% = +; 31 – 60% = ++; > 61% = +++